Numerical Investigations of Moist Rayleigh-Bénard Convection: A Study on Cloud Formation, Fluctuations, and Dynamic Modes

Zimu (Tim) Zhou (zz3645), Olivier Pauluis

Spring 2024

Contents

1 Abstract

This study utilizes Python's Dedalus Partial Differential Equation (PDE) solver to numerically solve the Boussinesq equations on High-Performance Computing (HPC) to investigate the dynamics of moist Rayleigh-Bénard convection. The computer simulations are conducted for Rayleigh-Bénard Convection in 2-dimensional (2D) and 3-dimensional (3D) spaces with different Rayleigh numbers, aspect ratios, and boundary conditions to explore their influence on cloud formation, fluctuation, and dynamic modes.

In the two-dimensional setting, the model is built on an x-z plane. By defining the y-components of the Boussinesq equations as separate scalar variables, the 2D model serves as a cross-sectional view of the regular 3D case with a significant conservation of computational cost. The computational analysis inspects the change of integrated kinetic energy, velocity components, and the square of velocity components on the simulated area to the normalized time scale under different Rayleigh numbers and resolutions. The specific shape of buoyancy, y-direction velocity, and liquid water content, as well as their correspondence when the surge of kinetic energy occurs, are examined by taking the contour plot of the variables at the corresponding time.

The 3D case is carried out in a cuboid with equal length and width much longer than its height. Similar to the 2D setting, this paper explores the effect of aspect ratio and Rayleigh number on the state of convection by looking into the contour plots and the change of the pivotal variables to the normalized time scale. Furthermore, this work applied Dynamic Mode Decomposition (DMD) to approximate the time evolution of variables and make future predictions.

2 Model Introduction

2.1 Dry Rayleigh-Bénard Convection

Rayleigh-Bénard convection is a usual phenomenon in thermodynamics that describes a specific pattern of cell-like convection within a fluid layer that is heated from below and cooled from above. Research on Rayleigh-Bénard convection is necessary to understand various natural processes, including atmospheric phenomena and oceanic circulation. The Rayleigh-Bénard convection is characterized by the spontaneous formation of convective cells when the temperature difference between the lower and upper boundaries exceeds a critical value due to buoyancy forces. The flow is characterized by Rayleigh Number (Ra), defined as the ratio of the time scale for diffusive thermal transport to the time scale for

convective thermal transport at speed u. Its formula is given by

$$Ra = \frac{g\beta}{\nu\kappa}(T_0 - T_H)H^3 \tag{1}$$

Where g is the gravitational acceleration, β is the thermal expansion coefficient, ν is the kinematic viscosity, and κ is the thermal diffusivity. We denote the height of the lower and upper boundary of the fluid layer to be 0 and H, respectively. Convection occurs when the Rayleigh Number exceeds a certain critical value.

2.1.1 Boussinesq-Navier-Stokes approximation

When studying the Rayleigh Bénard convection, we use the Boussinesq-Navier-Stokes approximation. This approximation allows for the description of the fluid flow dynamics in the presence of temperature gradients (or concentration gradients in the case of moist convection) without solving the full compressible Navier-Stokes equations. The momentum equation of Boussinesq-Navier-Stokes approximation of incompressible flow is given below:

$$\frac{d\mathbf{u}}{dt} = -\nabla p + \nu\nabla^2\mathbf{u} + Be_z \tag{2}$$

$$\nabla \cdot \mathbf{u} = 0 \tag{3}$$

The $\frac{d}{dt} = \frac{\partial}{\partial t} + \mathbf{u}\cdot\nabla$ denotes the material derivative, $\mathbf{u}$ is the velocity field, p is the kinematic pressure perturbation, and B is the buoyancy. Equation 3 means that the divergence of the velocity field is 0 everywhere. The physical meaning of 3 is that the local volume expansion is zero, and the flow of fluid is simply controlled by velocity.

2.2 Moist Rayleigh-Bénard Convection

When phase change is included in Rayleigh-Bénard convection, there are additional variables and equations to be considered in the model. The Moist Rayleigh-Bénard convection is primarily characterized by two Rayleigh numbers, Ra_M and Ra_D. They denotes the Moist Rayleigh Number and the Dry Rayleigh Number, respectively, and are defined as

$$Ra_M = \frac{(M_0 - M_H)H^3}{\nu\kappa}, \quad \text{and} \quad Ra_D = \frac{(D_0 - D_H)H^3}{\nu\kappa} \tag{4}$$

These equations quantify the buoyancy driving of the saturated and unsaturated buoyancy field M and D, respectively. Prandtl number is defined as the ratio of the kinematic viscosity to thermal diffusivity. Since the diffusivities for moist and dry buoyancy are the same,

there is only one Prandtl number, given by

$$Pr = \frac{\nu}{\kappa} \tag{5}$$

The Prandtl number is equal to 0.7 since we are interested in the convection in the atmosphere. The Reynold number is defined as the ratio of inertial forces and the kinematic viscosity, given by

$$Re = \frac{\|\mathbf{u}\|_2}{\nu} \tag{6}$$

The Boussinesq-Navier-Stokes approximation for the moist and dry buoyancy is given by

$$\frac{dM}{dt} = \kappa \nabla^2 M \tag{7}$$

$$\frac{dD}{dt} = \kappa \nabla^2 D \tag{8}$$

D and M are proportional to the liquid water potential temperature and to the equivalent potential temperature, respectively (Pauluis & Schumacher, 2010)[4]. By setting boundary conditions of D and M, we are controlling the heat at the boundary. Our model adopts the Kuo-Bretherton (KB) equilibrium for conditionally unstable atmospheres, given by

$$M_0 = D_0 \tag{9}$$

$$M_H = D_H - N_s^2 H \tag{10}$$

We also apply the free-slip boundary condition for the flow at both $z = 0$ and $z = H$. The Buoyancy B is defined as

$$B(D,\, M,\, z) = \max(M,\, D - N_s^2 z) \tag{11}$$

with the fixed Brunt-Väisälä frequency N_s that is determined by the moist adiabatic lapse rate. Water vapor begins to condense whenever $B = M$, as shown by the equation,

$$CW(D,\, M,\, z) = \max(0,\, M - D + N_s^2 z) \tag{12}$$

2.2.1 Rotational Moist Rayleigh-Bénard Convection

When the effect of the self rotation of Earth is considered in the Moist Rayleigh-Bénard Convection, the complete momentum equation becomes as follows:

$$\frac{d\mathbf{u}}{dt} = -fe_z \times \mathbf{u} - \nabla p + \nu\nabla^2\mathbf{u} + B(D,\, M,\, z)e_z \tag{13}$$

$$\nabla \cdot \mathbf{u} = 0 \tag{14}$$

$$\frac{dD}{dt} = \kappa\nabla^2 D \tag{15}$$

$$\frac{dM}{dt} = \kappa\nabla^2 M \tag{16}$$

$$B(D,\, M,\, z) = \max(M,\, D - N_s^2 z) \tag{17}$$

The $\frac{d}{dt} = \frac{\partial}{\partial t} + \mathbf{u}\cdot\nabla$ denotes the material derivative, $\mathbf{u}$ is the velocity field, p is the kinematic pressure perturbation, ν is the kinematic viscosity, κ is the thermal diffusivity, f is the Coriolis constant, B is the buoyancy, and D and M are dry and moist buoyancy, respectively. In the rotational scheme, the motion of air will be deflected by Coriolis Effect. The motion of airflow in the northern hemisphere will be deflected rightward. Specifically, hurricanes form because the convergent airflow at the bottom tends to rotate counterclockwise under the influence of the Coriolis force, while the divergent flow at the top similarly tends to rotate clockwise.

3 PDE Solver

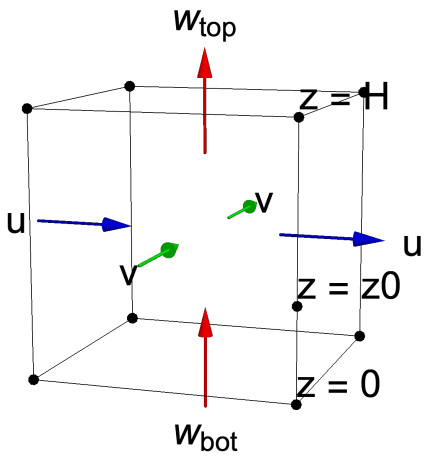

Figure 1: The simulated fluid layer

We use the PDE solver, Dedalus, to solve the Boussinesq-Navier-Stokes equations on Python to conduct computer simulations. In our simulations, the x- and y-basis are defined with real Fourier basis, such that we have periodic boundary conditions. By using periodic boundary conditions, we assume that the system repeats itself infinitely in horizontal directions. The real Fourier basis and incompressibility assumptions renders the vertical velocity integral over the cuboid truncated by $z = 0$ and any arbitrary $z = z_0$ in our simulation space to be equal to the mass flux over $z = z_0$. In particular. The proof is shown below. Pick any height $z = z_0$, we denote the cuboid bounded by $z = 0$, $z = z_0$, and the side surfaces as Ω. By Divergence Theorem, the total mass flux of Ω is given by

$$\int\int\int_{\Omega} \nabla \cdot \mathbf{u} \, dV \tag{18}$$

Equation 18 can be decompose to

$$\int_{z=z_0} w(z_0) \, d\mathbf{S} - \int_{z=0} w \, d\mathbf{S} + \int_{S_1} u \, d\mathbf{S} - \int_{S_2} u \, d\mathbf{S} + \int_{S_3} v \, d\mathbf{S} - \int_{S_4} v \, d\mathbf{S} \tag{19}$$

where we denote the right, left, front, and back boundaries as S_1, S_2, S_3, and S_4, respectively. The notation u, v, and w corresponds to figure 1. The integration over the side

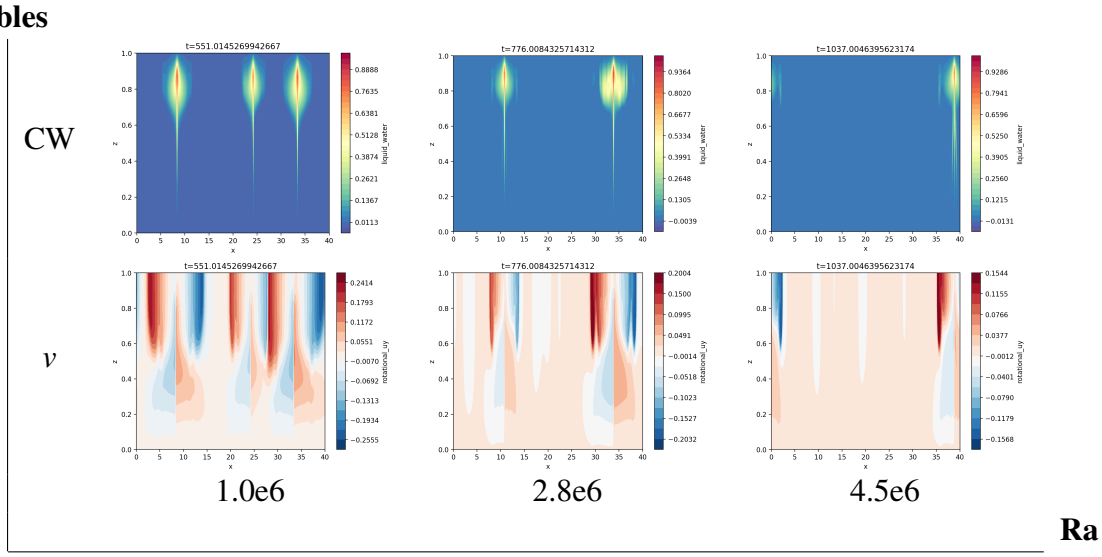

Table 1: Buoyancy and v when clouds begins to form, with resolution=32

surfaces are canceled due to the use of real Fourier basis, and the integration over the surface $z = 0$ equals to 0 since $w(z = 0) = 0$. The only term left is the first term of equation 19, which is the mass flux over $z = z_0$. In particular, if $z_0 = H$, then $w(z = 0) = 0$ and equation 19 equals to 0.

4 2d simulation

4.1 Visualization

In the 2d simulation defined on the x-z plane, all the vector fields on the x- and z-directions are well defined. The vectors in the y-direction in the 3d case are defined as scalar fields in our 2d simulations. Since the variables are all well-defined, we can treat the 2d simulation as a cross-sectional simulation of a 3d moist Rayleigh-Bénard convection. With $Pr = 1$, $M_H = -1$, and $D_H = \frac{1}{3}$, this paper explores the influence of Rayleigh number and resolution on cloud formation. We observe the cloud formation by adjusting the Rayleigh number as well as the vertical resolution of our simulation. The cloud formed in the 2d simulation does not change much with the Rayleigh number, but it shows a difference between different vertical resolutions.

By the definition of condensed water in Moist Rayleigh Bénard Convection, the liquid water content graphs in Table 1 and 2 indicate a high-buoyancy zone at the center of the

variables

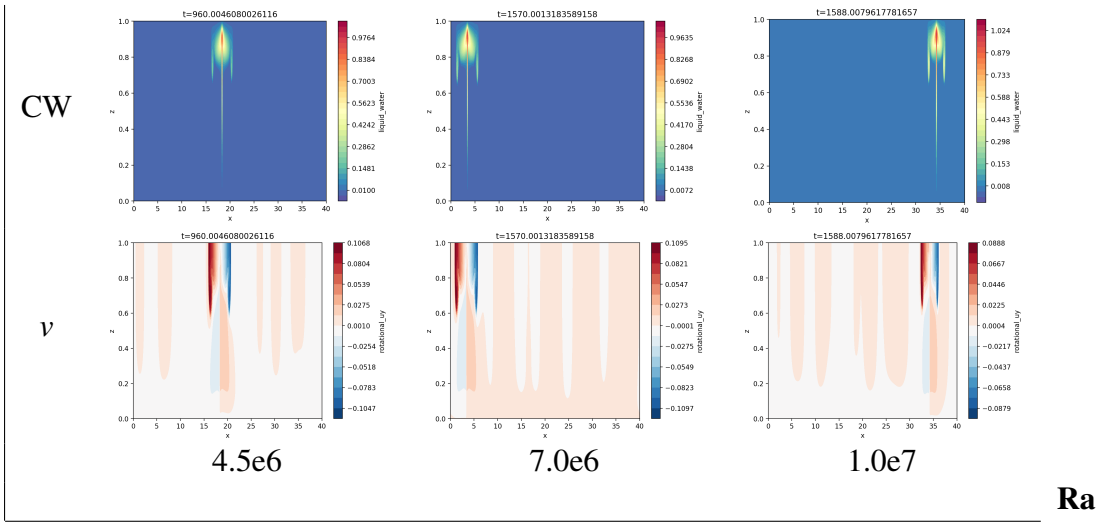

Table 2: Buoyancy and v when clouds begins to form, with resolution=64

clouds. This causes objects in the center of the cloud to move upward, resulting in a low-pressure zone at the bottom and a high-pressure zone at the top. The y-component velocity graphs, where positive value indicates the direction going into the page, demonstrate counterclockwise rotation at the bottom and the reverse at the top. Together, the figures in Table 1 and 2 agree with the dynamics of air under the Coriolis Effect in the norther hemisphere in reality.

4.2 Analysis

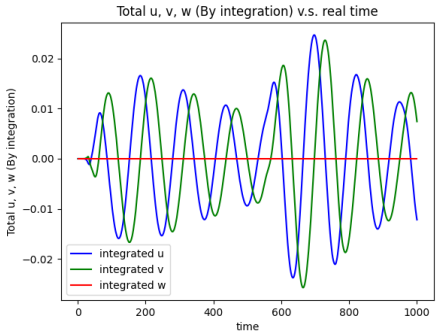

Figure 2: Integrated components of **u**

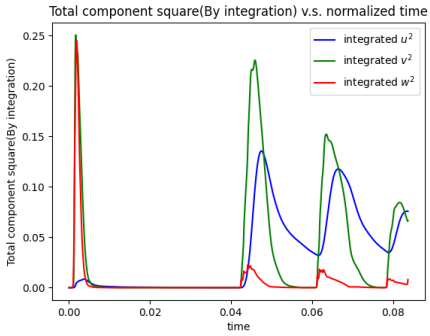

Figure 3: Integrated square of components of **u**

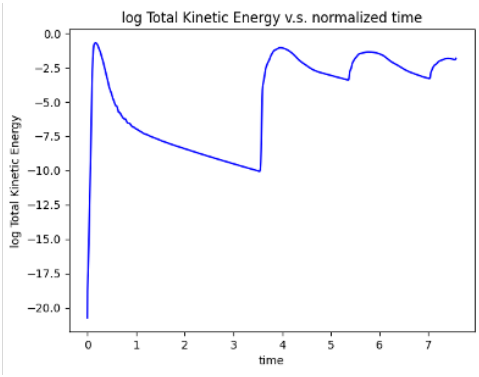

Figure 4: Logarithm of Kinetic Energy for Ra=1e6

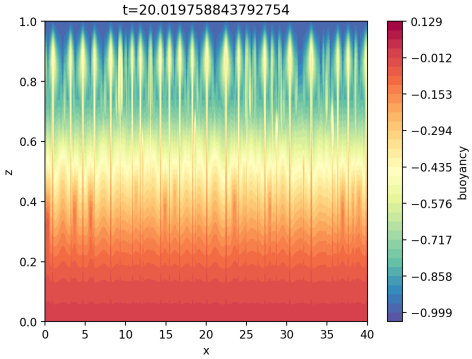

Figure 5: Shape of the first fluctuation in the simulation of Ra=1e6

The surge of kinetic energy shown in Figure 4 indicates the formation of clouds.
As discussed in Equation 19, the integration of the z-component of velocity is 0. The integration of the x- and y-components of velocity shows a periodic pattern, corresponding to Geostrophic Balance. By Equation 13, if we ignore all other terms except the Coriolis effect, then the momentum equation is component-wisely

$$\frac{du}{dt} = f * v \tag{20}$$

$$\frac{dv}{dt} = -f * u \tag{21}$$

The solution to the PDEs is a pair of trigonometric functions. In Figure 2, though the graph for u and v follow a trigonometric pattern, the amplitude decreases until the surge of kinetic energy. Figure 5 shows the simulation's buoyancy diagram for the first kinetic energy surge. As shown in Figure 3, the z-component of the velocity served as the dominant source of kinetic energy in the first surge, while that for the later surge are the x- and y-components. This phenomenon tells us that the fluctuation occurs as the beginning of the simulation occurs as vertical motions of the air parcel, whereas the cloud formation in later times is mainly composed of horizontal rotation in different layers.

5 3d simulation

Though the 2d simulations serve as a convenient cross-sectional view of the convection, 3d simulations give the comprehensive and realistic view of cloud formation. By conducting 3d simulation, this paper explores the relationship between the cloud formation and different parameters, including the moist Rayleigh number and aspect ratio.

5.1 Visualization

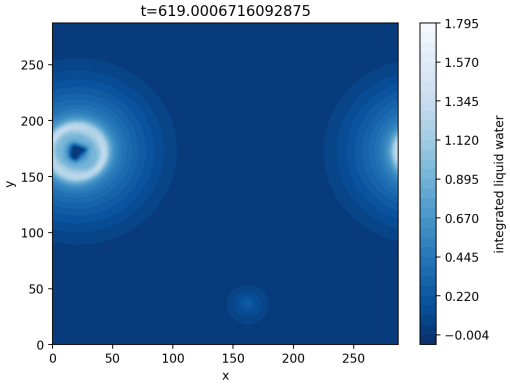

Figure 6: Vertical Integrated Liquid Water Content, A=9

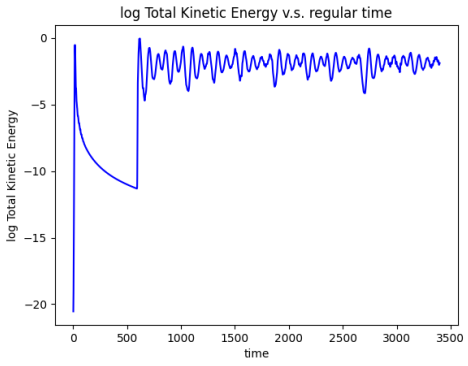

Figure 7: Integrated square of components of **u**

In 3d simulation, we began with non-rotating simulations of Moist Rayleigh Bénard Convection. As shown in Figure 6, the condensed liquid water forms a ring-shaped cloud. This corresponds to our conclusion of the 2d simulations. In fact, Figure 7 indicates the oscillating pattern of the formation of cloud.

5.2 Analysis

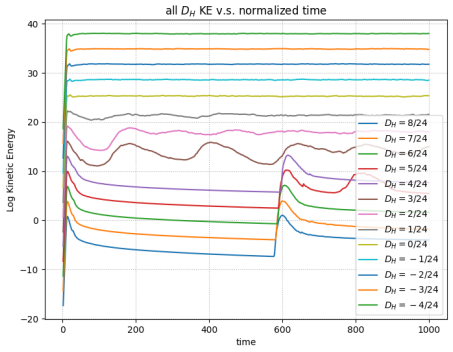

Figure 8: KE v.s. time under different boundary conditions, each vertically shifted by 3 for visibility

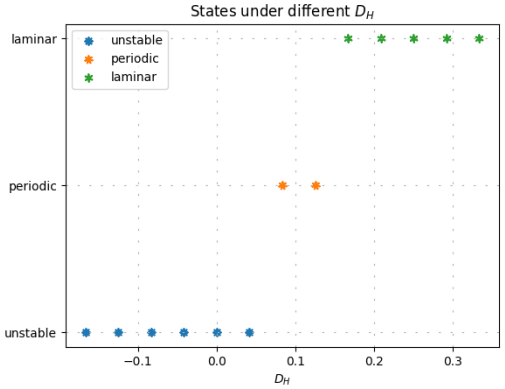

Figure 9: States v.s. D_H

To investigate the effect of different parameters on the convective states, we ran simulations with different boundary conditions D_H. These changes of D_H provide for different boundary heat conditions (e.g., adiabatic lapse rate) in the atmosphere in reality. We used D_H values ranging from -3/24 to 8/24, with 1/24 between each successive D_H. According to Figure 8, the cases where D_H below 1/24 stay at a completely unstable state throughout the simulation. When D_H is about 2/24 or 3/24, then there will be a nearly periodic convective state. If the D_H exceeds 4/24, the simulation will be at a laminar state, indicating a sudden burst after being silent for a long time.

6 Dynamic Mode Decomposition

6.1 DMD Algorithm

Dynamic Mode Decomposition (DMD) is a method of finding the pattern and make prediction for a given time series data. In Fluid Dynamics, we use DMD algorithm to approximate a time series data collected from a nonlinear dynamical system by a linear system. Usually, for a time series data for a given time T, $\{\mathbf{x_t}\}_{t=0}^{t=T}$, take

$$\mathbf{X} = [\mathbf{x_0} \cdots \mathbf{x_{T-1}}], \quad \mathbf{Y} = [\mathbf{x_1} \cdots \mathbf{x_T}] \in \mathbb{R}^{S \times T}$$

be two sets of data, where S denotes the dimension of each $\mathbf{x_t}$. Then we define matrix $\mathbf{A} = \mathbf{Y}\mathbf{X}^{\dagger}$, where $\mathbf{X}^{\dagger}$ denotes the peudo-inverse of $\mathbf{X}$. We can then use $\mathbf{A}$ to approximate

the motion by $\frac{d\mathbf{x}}{dt} = \mathbf{A}x$, or $\mathbf{Y} = \mathbf{AX}$. However, when n goes large, then this computation of $\mathbf{A}$ becomes unmanageable. Therefore, we may apply DMD algorithm to approximate $\mathbf{A}$ with lower cost. The DMD algorithm from [3] begins with taking the reduced singular value decomposition (reduced SVD) of $\mathbf{X}$; then use this SVD to compute $\mathbf{A}$.

$$\mathbf{X} = \mathbf{U}\Sigma\mathbf{V}^* \quad \Longrightarrow \quad \mathbf{A} = \mathbf{Y}\mathbf{V}\Sigma^{-1}\mathbf{U}^* \tag{22}$$

This gives us $A \in \mathbb{R}^{S\times S}$. In practice, denote $\Sigma \in \mathbb{R}^{r\times r}$, we take

$$\tilde{\mathbf{A}} = \mathbf{U}^*\mathbf{Y}\mathbf{V}\Sigma^{-1}$$

to be a further low-dimensional approximation that $\tilde{\mathbf{x}}_{\mathbf{k+1}} = \tilde{\mathbf{A}}\tilde{\mathbf{x}}_{\mathbf{k}}$, where $\tilde{\mathbf{x}}_{\mathbf{k}} = \mathbf{U}^*\mathbf{x}_{\mathbf{k}}$. By taking this $\tilde{\mathbf{A}}$, we can usually significantly reduce the computational cost for the following steps. Then, calculate the eigendecomposition of $\tilde{\mathbf{A}}$,

$$\tilde{\mathbf{A}}\mathbf{W} = \mathbf{W}\Lambda \quad \Longrightarrow \quad \mathbf{A}(\mathbf{UW}) = (\mathbf{UW})\Lambda \tag{23}$$

Therefore, the eigenvectors of $\mathbf{A}$ and $\tilde{\mathbf{A}}$ are given by columns of $\mathbf{UW}$ and $\mathbf{W}$, respectively. Since $\mathbf{U}$ is the left singular vectors of $\mathbf{X}$, $\mathbf{UW}$ lies on the range of $\mathbf{X}$. For better capturing the shift from $\mathbf{X}$ to $\mathbf{Y}$, we take

$$\Phi = \mathbf{AUW} = \mathbf{Y}\mathbf{V}\Sigma^{-1}\mathbf{W}$$

to be the eigenvector of $\mathbf{A}$. This approach aligns the right singular vectors and singular values of $\mathbf{X}$ with the temporal dynamics represented in $\mathbf{Y}$.
After calculating the DMD, we can select an arbitrary initial condition $\mathbf{x_i}$, and timestep Δt. Compute the initial amplitude $b = \Phi^{\dagger}\mathbf{x_i}$ and rewrite $\Omega = \frac{\log\Lambda}{\Delta t}$, then the approximate solutions is given by

$$\mathbf{x}(t) = \Phi\exp(\Omega t)\mathbf{b} \tag{24}$$

Since the eigenvalues stored in Λ all have norm less than or equal to 1, by Equation 24, the $\mathbf{x}(t)$ captured by DMD decays exponentially with time. The eigenvalues with the largest norm determines the time evolution captured by DMD.

6.2 Application and Results

We apply DMD on the time series data of moist buoyancy.

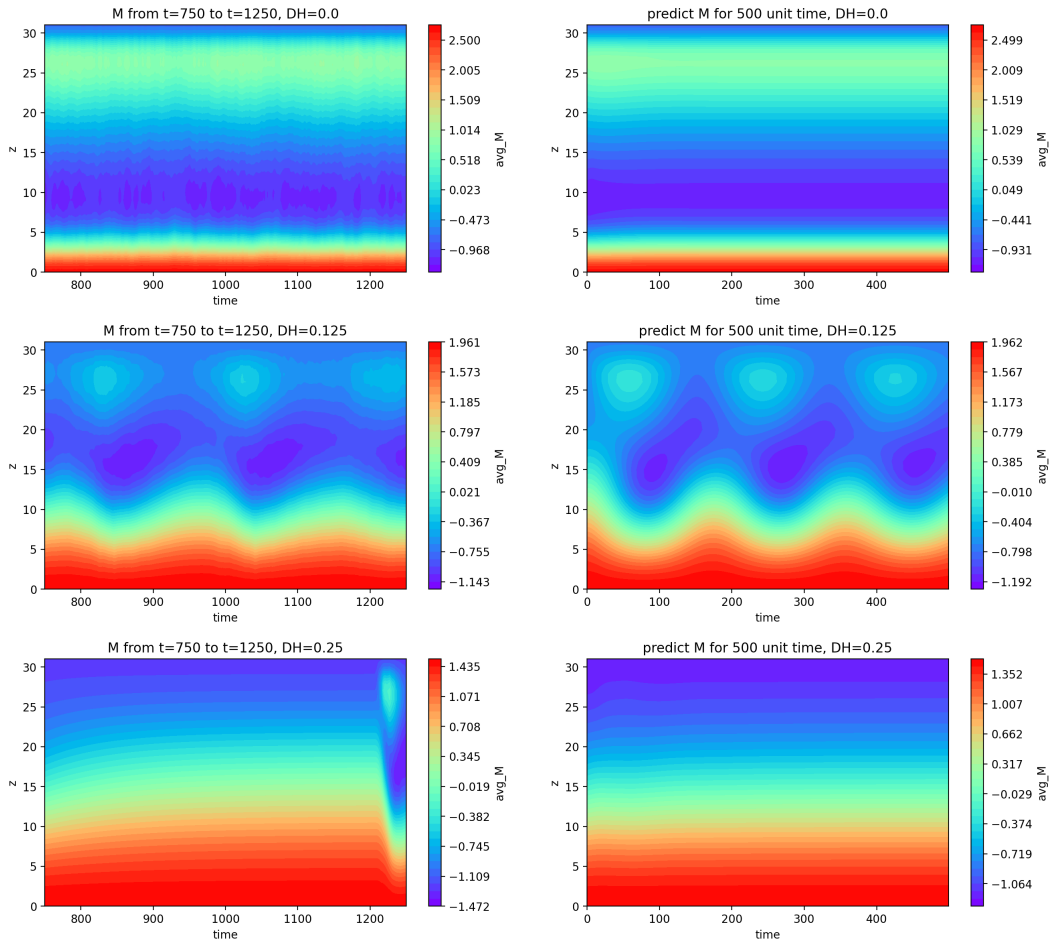

Figure 10: The visualization of the time series data of M and the dynamic mode captured by DMD of cases D_H =0/24, 3/24, and 6/24

Figure 10 is displaying the time series data of moist convection on the left and the prediction made by DMD on the right, each in a time scale of 500 unit time in the simulation. This figure suggests that DMD is unable to capture small and frequent fluctuations or sudden bursts, but can do well at capturing large and general trends.
In some of the cases which end up with laminar state, the prediction made by DMD blows up. This is caused by the high condition number of the data due to extreme values. When the condition number is high, the probability of rounding error will be very high. Therefore, the norm of the eigenvalues stored in Λ will sometimes be greater than 1, which makes the prediction to blow up.

7 Conclusion

Rayleigh Bénard Convection explains that natural convection occurs in an atmospheric layer with heating at the bottom and cooling at the top. By considering vapor condensation, the Moist Rayleigh Benard Convection is more accurate but complex than the traditional model. The Moist Rayleigh Bénard Convection uses dry and moist buoyancy to represent the heat at the boundaries, and these variables render two more differential equations to the Boussinesq equations of the dry convection model. Together with the momentum equation, assumption of incompressibility, and initial and boundary conditions, the moist model provides a more nuanced understanding of atmospheric and oceanic processes, particularly in predicting weather patterns and studying environmental systems.

Introducing the Coriolis Effect, our model considers the effect of Earth's self-rotation on the state of convection. This adjustment leads to a more accurate representation of real-world atmospheric phenomena, such as cyclonic movements.

When solving the Boussinesq equations, the efficiency of our solver, Dedalus, provides a concrete foundation for the success of the computer simulation of the moist model. The choice of numerical methods and boundary conditions crucially influences the stability and accuracy of the simulations, reflecting the delicate balance required in computational fluid dynamics. The simulations demonstrate the influence of various parameters—such as the Rayleigh number, aspect ratio, and boundary conditions—on the convection state.

The 2D simulations, with the third component of velocity defined as a scalar variable, provide a cross-sectional view of the standard 3D simulation. All the simulations show an oscillatory pattern in the integrated x- and y-component of velocity, revealing geostrophic balance. The shapes of the clouds formed are similar in the simulations under different Rayleigh Numbers. However, within each of the simulations, the first convection, dominated by the vertical motion of objects, has a different convection pattern than that of the subsequent cloud formations where horizontal rotation is significant.

On the other hand, the 3D simulations demonstrate the sharp change of convective states and the change of boundary conditions. With different D_H and other parameters remaining the same, we observe that there appear to be three kinds of convective states: unstable, periodic, and laminar state. Lower D_H's maintain a continuous convective state, while higher D_H prompt transitions to a laminar state, highlighting the parameter's critical role in defining the system's dynamic state. Since the D_H in the moist model defines the heating boundary condition at the top of the simulated layer, our result suggests a sensitive dependence on geometric and thermal inputs.

Dynamic Mode Decomposition (DMD) provided a powerful tool for analyzing the time-

series data generated by our simulations, enabling the extraction of dominant modes and predicting future states. The application of DMD highlighted its utility in capturing the system's essential dynamics while ignoring small fluctuations and sudden bursts. This not only helps us accurately capture the most critical information about the system's fundamental dynamics but also illustrates the usefulness of DMD in fluid dynamics.

References

[1] Chien, M.-H., Pauluis, O. M., & Almgren, A. S. (2022). Hurricane-like vortices in conditionally unstable moist convection. *Journal of Advances in Modeling Earth Systems*, 14, e2021MS002846. https://doi.org/10.1029/2021MS002846

[2] Keaton J. Burns et al. Dedalus: A flexible framework for numerical simulations with spectral methods. In: *Phys. Rev. Res.* 2 (2 Apr. 2020), p. 023068. doi: 10.1103/PhysRevResearch.2.023068. url: https://link.aps.org/doi/10.1103/PhysRevResearch.2.023068.

[3] Kutz, Jose Nathan et al. Dynamic Mode Decomposition *Philadelphia : Society for Industrial and Applied Mathematics*, 2016

[4] Pauluis, O. M., & Schumacher, J. (2010). *Idealized moist Rayleigh-Benard convection with piecewise linear equation of state.* Communications in Mathematical Sciences, 8(1), 295–319. https://doi.org/10.4310/CMS.2010.v8.n1.a15